

CHEMISTRY

AN ASIAN JOURNAL

www.chemasianj.org

Accepted Article

Title: Ferroelectric Liquid Crystals: Synthesis and Thermal Behavior of Optically Active, Three-Ring Schiff bases and Salicylaldehydes

Authors: Channabasaveshwar Veerappa Yelamaggad, Bhyranalyar N Veerabhadraswamy, and Doddamane S Shankar Rao

This manuscript has been accepted after peer review and appears as an Accepted Article online prior to editing, proofing, and formal publication of the final Version of Record (VoR). This work is currently citable by using the Digital Object Identifier (DOI) given below. The VoR will be published online in Early View as soon as possible and may be different to this Accepted Article as a result of editing. Readers should obtain the VoR from the journal website shown below when it is published to ensure accuracy of information. The authors are responsible for the content of this Accepted Article.

To be cited as: *Chem. Asian J.* 10.1002/asia.201800119

Link to VoR: <http://dx.doi.org/10.1002/asia.201800119>

A Journal of



A sister journal of *Angewandte Chemie*
and *Chemistry – A European Journal*

WILEY-VCH

Ferroelectric Liquid Crystals: Synthesis and Thermal Behavior of Optically Active, Three-Ring Schiff bases and Salicylaldimines

Bhyranalyar N. Veerabhadraswamy, D. S. Shankar Rao and C. V. Yelamaggad

Centre for Nano and Soft Matter Sciences

P. B. No. 1329, Prof. U. R. Rao Road, Jalahalli, Bengaluru 560013, India

*Tel: +91-80-2308 4233; Fax: 91-80-28382044; E-mail: yelamaggad@cens.res.in/
yelamaggad@gmail.com.*

Abstract: Chiral ferroelectric smectic C* (SmC*) phase, characterized by a helical superstructure, has been well exploited in developing high-resolution microdisplays that have been effectively employed in the fabrication of a wide varieties of portable devices. Although, an overwhelming number of optically active (chiral) liquid crystals (LCs) exhibiting SmC* phase have been designed and synthesized, the search for new systems continues so as to realize mesogens capable of meeting technical necessities and specifications for their end-use. In continuation of our research work in this direction, herein we report the design, synthesis and thermal behavior of twenty new optically active, three-ring calamitic LCs belonging to four series. The first two series comprise five pairs of enantiomeric Schiff bases while the other two series are composed of five pairs of enantiomeric salicylaldimines. In each pair of optical isomers the configuration of a chiral centre in one stereoisomer is opposite to that of the analogous centre in the other isomer as they are derived from (3*S*)-3,7-dimethyloctyloxy and (3*R*)-3,7-dimethyloctyloxy tails. To probe the structure-property correlations, in each series, the length of the *n*-alkoxy tail situated at the other end of the mesogens has been varied from *n*-octyloxy to *n*-dodecyloxy. The measurement of optical activity of these chiral mesogens was carried out by recording their specific rotations. As expected, enantiomers rotate plane polarized light in the opposite direction but by the same magnitude. The thermal behavior of the compounds was established using a combination of optical polarizing microscopy, differential scanning calorimetry and powder X-ray diffraction. These complementary techniques evidence the existence of the expected, thermodynamically stable, chiral smectic C (SmC*) LC phase besides blue phase-I/II (BPI or BPII) and chiral nematic (N*) phase. However, as noted in our previous analogous study, the vast majority of the Schiff bases show an additional metastable, unfamiliar smectic (SmX) phase just below the SmC* phase. Notably, the SmC* phase persists over the temperature span of ~ 80-115 °C. Two mesogens chosen each from Schiff bases and salicylaldimines were investigated for their electrical switching behavior. The study reveals the ferroelectric switching characteristics of the SmC* phase featuring the spontaneous polarization (P_S) in the range of 69 to 96 nC/cm². The helical twist sense of the SmC* phase as well as the N* phase formed by a pair of enantiomeric Schiff bases and salicylaldimines has been established with the help of circular dichroism (CD) spectroscopic technique. As expected, the SmC* and the N* phase of a pair of enantiomers showed mirror imaging CD signals. Most importantly, the reversal of helical handedness from left to right and vice-versa has been evidenced during the N* to SmC* phase transition implying that the screw sense of the helical array of the N* phase and the SmC* phase of an enantiomer is opposite.

I. Introduction

As is well known, chirality, the lack of mirror symmetry of an object existing in two non-superimposable mirror image (enantiomeric) forms, is ubiquitous in nature which exists in a wide variety of systems of all length scales say from elementary particles to mesoscopic / macroscopic structures.¹⁻³ Most importantly, it plays a vital role in self-assembly / self-organization of functional molecular materials. In fact, chiral materials capable of transmitting chirality from molecular level to the macroscopic scale are well-known to possess special characteristics that have great significance in both basic research and practical applications. For example, optically active shape-anisotropic molecules, called chiral mesogens, self-assemble spontaneously upon heating into liquid crystal (LC) phases which are not only anisotropic fluids but also display exceptional chiral bulk properties inherently.⁴⁻⁸ Precisely, the self-assembly of chiral mesogens leads to the formation of frustrated phases and helical superstructures in addition some chiral layered structures. Indeed, such phases can also be realized effectively by doping LC phases formed by achiral mesogens (hosts) with chiral dopants (guests) with chiral materials, which need not be necessarily be liquid crystalline in nature. The twist grain boundary (TGB) phases and blue phases (BPs), being highly frustrated phases with lattice defects originating from the competition between the chiral twisting force and the urge of mesogens to pack in certain manner so as to fill the space uniformly, have been attracting attention due to their fascinating physical features and structural complexity. The defect free helical superstructures such as chiral nematic (N*) and chiral smectic C (SmC*) phases, resulting from the handedness interactions leading to the twisted arrangements of the constituent chiral mesogens, have been demonstrated to be potentially promising candidates for present and many advanced technological endeavors.⁶⁻¹¹ For example, the SmC* phase exhibiting ferroelectric polarization switching holds a great potentiality for large-scale applications in flat panel displays featuring high image quality, fast response time (micro-seconds), optical bistability, high resolution and wide-viewing angles.⁶⁻¹³ Therefore, the mesogenic materials, including supramolecular (self-complimenting) motifs,¹⁴ exhibiting this phase, generally referred to as ferroelectric liquid crystals (FLCs), have been ~~the~~ attracting particular attention of many technologists as well as basic researchers because they provide additional advantages when compared to classical LC displays (LCDs) derived from the nematic (N) LC materials.⁶⁻³⁵ For example, the switching time of FLC displays can be 1000 times faster than the twisted nematic devices.

The ferroelectric property of the SmC* phase stems, in fact, from the chirality directed self-assembly of the constituent rod-like mesogens in a particular manner. Enantiomerically enriched rod-like mesogens align parallel to each other to form diffuse layers wherein the mesogens (along their long molecular axis, director, \mathbf{n}) in each layers tilt at an angle with respect to the layer normal. The tilt angle, being nearly identical in all layers, shows temperature dependence that generally increases upon lowering the temperature. Thus, needless to say, the tilt orientational ordering among the succeeding layers persists over long distances. Owing to the presence of chiral mesogens in high enantiomeric excess, the director (\mathbf{n}) adopts helical macrostructure with a characteristic pitch. That is, a helicoidal structure results due to a gradual change in the tilt direction of constituent mesogens from layer to layer, about an axis perpendicular to the layer planes. Indeed, the chirality of the constituent mesogens determines the sense of rotation of a helicoidal structure that can be either left-handed or right-handed. Given the fact that the tilted mesogens are chiral, the local symmetry reduces to a two-fold axis of rotation; this scenario creates inequivalence in the dipole moment along the C_2 axis of layers leading to spontaneous polarization (P_s) in each layer. Accordingly, the P_s averages out to zero and therefore, the bulk SmC* phase is defined as 'helielectric'. However, a macroscopic polarization can be achieved by unwinding the helix with the aid of external forces such as an electric field or shear or by surface interactions and thereby the bulk SmC* phase becomes ferroelectric. The molecular tilt coupled with chirality enforces the layers to be polar and the polarity can be switched by the application of an electrical field. This behavior of the SmC* phase has been well exploited in the development of advanced display devices featuring the outstanding characteristics discussed earlier.⁶⁻¹³

However, for the end-use in a range of devices the ferroelectric LC materials should possess certain important physical properties.⁶⁻¹³ First and foremost, the materials should show the ferroelectric SmC* phase over a wide temperature range say from subambient (−30 °C) to high temperature (80 °C). The chemical (heat and moisture) stability as well as resistance to light are absolutely essential. The birefringence, viscosity, molecular tilt angle, etc. are the other necessities of materials. The successful fabrication of devices, where the alignment of constituent mesogens is important, the FLC material should display the N*and/or SmA phases (preferably over a narrow temperature range) above the SmC* phase existing for a wide thermal width. Above all, the P_s value of material, to be used for the device fabrication, is one of the crucial factors. The experimental results accumulated hitherto

suggest that the magnitude of P_S depends not only on the molecular tilt angle but also on the dipole at the chiral centre.¹⁴ The P_S value diminishes if the rotation of chiral centre, besides other intramolecular rotations, around the long molecular axis is high. Lowering the distance between chiral carbon atom and the position of the molecular transverse dipole is the one of the ways of controlling the negative impact of intramolecular rotations. In other words, the hindered rotation of a chiral moiety with respect to core helps in enhancing the strength of P_S .^{13,14} These aspects signify the importance of the coupling between the dipole at the chiral centre and the dipoles of the molecule.^{13,14}

In view of these thought-provoking observations and in a quest to achieve superior FLCs for display devices, we have recently investigated four series of three-ring calamitic LCs (Schiff bases and salicylaldimines) comprising imine (-CH=N-) and ester (-COO-) linking groups and (*S*)-2-octyloxy and (*R*)-2-octyloxy chiral tails (Chart 1).^{36,37} In these mesogens, while the linking groups, needless to say, induce lateral polarity, the chiral tails, where the chiral centre resides closer to the core, not only induce molecular chirality but also account for the hindered rotation of a chiral carbon centre. Notably, these compounds displayed, besides BPs and N* phase, a thermodynamically stable ferroelectric SmC* phase over a 50–70 °C thermal width with P_S value of about 100 nC/cm².^{36,37} To validate the dependence of P_S magnitude on the position (rotation) of chiral centre, we intended to incorporate (3*S*)-3,7-dimethyloctyloxy and (3*R*)-3,7-dimethyloctyloxy tails in the molecular design of three-ring calamitic LCs reported by us earlier.^{36,37} Precisely, in the present study we intended not only to know the effect of locating the chiral centre far from the three-ring core but also to understand the overall structure-property correlations. Herein we report the synthesis, the molecular structural characterization and phase transitional behavior of twenty new optically active three-ring calamitic LCs, Schiff bases and salicylaldimines, that are substituted terminally with (3*S*)-3,7-dimethyloctyloxy or (3*R*)-3,7-dimethyloctyloxy tail. The general molecular structures of five pairs of enantiomeric Schiff bases (Series-I and II) and five pairs of enantiomers derived from salicylaldimine-core (Series III and IV) are shown in Scheme-I. As can be seen, in any given pair of optical isomers (enantiomers) the configuration of a chiral centre in one isomer is opposite to that of the analogous centre in the other isomer as they are derived from (3*S*)-3,7-dimethyloctyloxy and (3*R*)-3,7-dimethyloctyloxy tails. To investigate the relationship between molecular structure and LC behavior, the length of the *n*-alkoxy tail situated at the other end of the mesogens has been varied from *n*-octyloxy to *n*-dodecyloxy. For the convince, the acronyms used for referring

these four series of mesogens in the entire text are **SB(3S)-n** (Series-I), **SB(3R)-n**, (Series-II), **SA(3S)-n** (Series-III) and **SA(3R)-n** (Series-IV) where **SB**, **SA** and **n** denote Schiff bases, salicylaldehyde and number of carbon atoms in the terminal tail respectively; (**S**) and (**R**) indicate the absolute configuration of chiral tail.

II. Results and discussion

II.1. Synthesis, molecular structural characterization

The target, optically active mesogens belonging to four series, viz., Series-I: **SB(3S)-n**, Series-II: **SB(3R)-n**, Series-III: **SA(3S)-n** and Series-IV: **SA(3R)-n**, were synthesized in excellent (80-86 %) yields by following conventional synthetic steps shown in Scheme-I. (3S)-1-((3,7-Dimethyloct-6-en-1-yl)oxy)-4-nitrobenzene (**1**) and (3R)-1-((3,7-dimethyloct-6-en-1-yl)oxy)-4-nitrobenzene (**2**) were prepared by the O-alkylation of 4-nitrophenol respectively with (*S*)-(+)-citronellyl bromide and (*R*)-(-)-citronellyl bromide in the presence of a mild base (anhydrous K₂CO₃), in butanone, and KI as catalyst. The subsequent catalytic hydrogenation at room temperature under 1 atm of H₂ (balloon) in the presence of 10 % Pd/C (5 wt%) of compounds **1** and **2** gave the corresponding anilines viz., (*S*)-4-((3,7-dimethyloctyl)oxy)aniline (**3**) and (*R*)-4-((3,7-dimethyloctyl)oxy)aniline (**4**). The key intermediates namely, 4-formylphenyl 4-(*n*-alkoxy)benzoates (**7a-e**) and 4-formyl-3-hydroxyphenyl 4-(*n*-alkoxy)benzoates (**8a-e**) were obtained respectively in good yields by the esterification of 4-(*n*-alkoxy)benzoic acids (**6a-e**) with 4-hydroxybenzaldehyde and 2,4-dihydroxybenzaldehyde in the presence of dicyclohexylcarbodiimide (DCC) and 4-dimethylaminopyridine (DMAP) as catalyst. In turn, compounds **6a-e** were prepared by subjecting 4-(*n*-alkoxy)benzaldehydes (**5a-e**) to Jones oxidation; the latter aldehydes (**5a-e**) were synthesized by performing Williamson ether synthesis wherein 4-hydroxybenzaldehyde was treated with *n*-bromoalkanes. In the final reaction, the aldehydes **7a-e** and **8a-e** were condensed with anilines **3** and **4** to obtain Schiff bases [Series-I: **SB(3S)-n**; Series-II: **SB(3R)-n**] and salicylaldehydes [Series-III: **SA(3S)-n** and Series-IV: **SA(3R)-n**] in notable yields. The details of the synthetic procedures together with the characterization data of the target mesogens and intermediates are given in the experimental section and supporting information respectively.

All twenty final compounds have been fully-characterized with the help of elemental analyses as well as spectroscopic techniques such as UV-visible, FTIR, ¹H NMR, ¹³C NMR

and FAB Mass (see Supporting Information: **Figs.S1 to S40**). Given the fact that the vast majority of the intermediates are known, their molecular structures have been ascertained by FTIR, ^1H NMR and FAB Mass spectroscopic techniques only. The characterization data were found to be consistent with the proposed structures of all the compounds synthesized during the present study. The optical purity of the chiral mesogens was determined by measuring the specific rotation. The magnitude of the specific rotation measured for a pair of enantiomers found to be the same but in opposite direction.

II.2. Evaluation of liquid crystal behavior

Liquid crystal behavior of all the four series of mesogens (two series of Schiff bases and two series of salicylaldimines) realized was systematically examined using two conventional complimentary techniques viz., polarizing optical microscopy (POM) and differential scanning calorimetry (DSC). The individual mesophases were identified based on the characteristic textural pattern shown by them under POM. The phase sequences of the mesogens were established by carefully noticing the change in the textural pattern while passing from one mesophase to another. The phase transition temperatures and associated enthalpies were determined from the DSC traces recorded, at a rate of $5\text{ }^\circ\text{C} / \text{min.}$, during the first heating and cooling cycles. In case when the signatures are not seen in DSC thermograms, the phase transition temperatures noted during the POM study are taken for presentation. Powder X-ray diffraction (XRD) and electrical switching experiments have been carried out on a few randomly selected samples. Table 1 and 2 depict the thermal behavior of the Schiff bases [Series-I: **SB(3S)-n**; Series-II: **SB(3R)-n**] and salicylaldimines [Series-III: **SA(3S)-n** and Series-IV: **SA(3R)-n**] respectively. As can be seen from the accumulated results, all the Schiff bases and salicylaldimines display enantiotropic mesomorphism. In particular, Schiff bases, **SB(3S)-n** and **SB(3R)-n** series of mesogens, show three mesophases that were clearly identified as BPI/II, N^* and SmC^* phases; however, all the members, except for a pair of enantiomers (see Table 1 and the following discussion), exhibit an additional metastable LC phase just below the SmC^* phase. The characteristics of this metastable phase being unfamiliar, hereafter it will be referred to as SmX phase. The salicylaldimines, **SA(3S)-n** and **SA(3R)-n** series of mesogens, display BPI/II, N^* and SmC^* phases. In the following sections we describe how these LC phases were identified and the ferroelectric properties of the SmC^* phase was established.

II.2.1. Polarized light microscopy and calorimetric studies

The thin films of the samples, prepared by placing a tiny amount of mesogens between clean (untreated) glass slides, upon slow ($0.2\text{ }^{\circ}\text{C / min}$) cooling from isotropic liquid state, show the growth of striking deep blue, micron sized platelets emanating from the dark background (Fig. 1a); on cooling the sample further, a platelet texture composed of light (sky) blue, deep blue and green plates quickly grows filling the entire field of view (Fig. 1b). If the film is subjected to gentle mechanical stress the Grandjean plane texture of the N^* phase appears. It is well known that the cubic BPI and BPII phases, composed of double twist cylinders, possess 3D orientational ordering with periods nearly equal to 500 nm that is of the order of the wavelength of visible light. Therefore, they Bragg-scatter light in the visible range. They generally comprise differently oriented domains of different colors giving rise to the textural pattern characterized by a mosaic of varying colors. Thus, the textural pattern seen under the POM suggests the existence of a cubic blue phase which can be either BPI or BPII.³⁸ It may be mentioned here that the signature/peak due to I-BP transition could not be detected in DSC thermograms. On lowering the temperature further from the BPI/II phase, a transition to a single twist phase, the N^* phase occurs with a focal conic / fan-shaped texture (Fig. 1c) where a random ordering of the helix exists. In fact, due to slow cooling of the sample, the focal conic pattern growing into the platelet texture of BPI/BPII texture could be seen. When the fan-like texture was subjected to a shearing test (mechanical stress), the oily streaks characteristics of the Grandjean plane texture (Fig. 1d) occur where the helix axis remains perpendicular to the glass plates, i.e. along the viewing direction. Further cooling the N^* phase, a transition to the SmC^* phase occurs. During this transition, the fan-shaped texture of the N^* phase sharply transforms into a textural pattern composed of both broken focal-conics superimposed by the equidistant (dechiralization) lines and a dull-grayish cloudy (low birefringent) pattern (Fig. 1e) stemming respectively from the homogeneous and homeotropic alignment of the constituent mesogens. When examined in slides treated for planar orientation, the SmC^* phase displayed, as expected, a texture featuring an equidistant line pattern on top of fans implying the pitch of the helix is in the order of several micrometers; as a representative case, a microphotograph of such a texture seen for the mesogen **SA(3R)-10** at $152.4\text{ }^{\circ}\text{C}$ is shown Fig. 1f.

Thus, optical textural observation evidence the occurrence of enantiotropic mesophases such BPI/II, N^* and SmC^* phases in both Schiff bases and salicylaldimines.

However, as discussed earlier, all the Schiff bases, except for a pair of enantiomers **SB(3S)-9** and **SB(3R)-9**, show an additional metastable LC phase, the SmX phase, below the SmC* phase. On further cooling these mesogens from the SmC* phase with the textural pattern shown in Fig. 1e, a sharp transition to the SmX phase results that was evidenced by the observation of a textural pattern comprising the *pseudo*-isotropic regions as well as ill-defined birefringent domains (Fig. 1g). Notably, if the sample is cooled from the planarly oriented SmC* phase, the SmX phase shows an uncharacteristic textural pattern where a line pattern persists over the dull long fans (Fig. 1h). However, as we shall discuss later, XRD studies suggest the SmX phase being a tilted hexatic phase. As shown in Figs. S41a and S41b, the DSC traces obtained respectively for a member of Schiff base series and that of a salicylaldimine series, as representative cases, corroborated the results derived from the textural pattern study using POM. The plots of transition temperatures as a function of the terminal *n*-alkoxy chain length for the Schiff bases and salicylaldimines are shown in Figs 2a and 2b respectively. It can be immediately seen that the clearing temperatures decrease as the length of the alkyl tail increases. The thermal range of BPI/II, being extremely small, appears to be arbitrary (see the expanded versions of Figs 2a and 2b) as has been adjudged by the microscopic study. The thermal width of N* phase decreases upon increasing the length of *n*-alkoxy tail. Likewise, in general, the temperature range of the SmC* phase shrinks when the length of *n*-alkoxy tail is increased.

II.2.2. Powder X-ray diffraction study

As discussed earlier, the director in the Smectic C* phase tilt at an angle with respect to the layer normal and it is the precession of the tilt around the layer normal constitutes macroscopic helical structure of the phase. In fact, this can be easily figured out with the help of XRD study where the measured spacing (*d*) is smaller than the molecular length (*L*) of the mesogens in their all-*trans* conformation. Thus, XRD experiments were carried out on four samples, **SB(3S)-8**, **SB(3S)-12**, **SA(3S)-8** and **SA(3R)-12**, two representative mesogens chosen from each Schiff base and salicylaldimine series. The samples were filled by capillary action into Lindemann capillary (1 mm diameter) tubes in the isotropic phase. The capillaries were flame-sealed at each end carefully so that the samples to be investigated are not heated / burnt. While cooling the samples, the diffraction patterns were recorded as a function of temperature in the region of SmC* phase. The profiles acquired at different temperatures found to be virtually indistinguishable. Figures 3a and 3b show the 1D intensity vs diffraction

(2θ) profiles obtained at different temperatures that were found to be nearly the same, as expected. Table 3 gives the spacings (d) corresponding to the low-angle reflections and the wide-angle peak positions, as well as d/L ratio where L is the estimated all-*trans* molecular length determined from the MM2 calculation of Chem3D molecular model; the Table 3 also lists tilt angle (θ) of the mesogens.

Each profile shows a diffuse scattering maximum in the wide-angle region ($2\theta \approx 20^\circ$) and a sharp peak corresponding to the layer thickness d , in the small angle region ($0 < 2\theta < 5^\circ$) suggest the mesophase being a smectic phase. The diffuse nature of the wide angle peak indicates a liquid like in-plane order; that is, this broad peak stems from the inter-molecular separation within the smectic layer arising due to the liquid-like positional correlation within the layer. As shown in Table 3, the d values are lower than the estimated all-*trans* molecular length (L) of the mesogens estimated from the energy minimized conformation with the methylene units in the fully extended form in the all-*trans* conformation. As mentioned earlier the d/L ratio are less than one implying the tilted organization of the molecules within the smectic layers. The tilt angle (θ) of the mesogens with respect to the layer normal, estimated using the expression $\theta = \cos^{-1}(d/L)$, was found to be in the range of 41.4 - 50.2 (see Table 3). As expected, the d value decreases on cooling the phase pointing to a fact that the tilt angle of the molecules within the smectic layers increases upon reducing the temperature (Table 3). Thus, the XRD data together the optical textural pattern observed corroborate the occurrence of the SmC* phase.

II.2.3. Electrical switching investigation

In order to reveal the ferroelectric behavior, the SmC* phase stabilized by the mesogens, **SB(3S)-8** and **SA(3R)-11**, as a representative case each from Schff base and salicylaldimine series of compounds, was subjected to electric field experiments. As mentioned before, due to the reduced C_2 symmetry and tilting of the mesogens the P_s in the plane of each layer, averages out to zero due to the intrinsic helical structure of the SmC* phase. However, a macroscopic P_s can be obtained by simply unwinding the helix of the phase with the help of an external stimulus such as electric field.

The requisite cells were locally constructed using glass slides coated with indium tin oxide (ITO) that were initially treated with a polyimide solution and unidirectionally so that

the molecules orient planarly. The samples, in their isotropic liquid state, were drawn into cells (by capillary action) and cooled slowly in to the SmC* phase and measurements were performed with a triangle waveform. After cooling the sample **SB(3S)-8** from isotropic state to the SmC* phase and holding at 129 °C, a low frequency AC triangular-wave voltage was applied and then increased slowly. As shown in Fig. 4a, a single polarization current peak for each half period appears at a voltage of 145.3 V (51.3 Vrms) and a frequency of 5 Hz, (09 kΩ). Notably, the results could be reproduced for any number of times vouching for the stability of the mesogen. In fact, the peak observed in the mesophase vanished on going to the N* phase or isotropic phase, ruling out the possibility of ionic contribution. The P_s value estimated from this trace is about 69 nC cm⁻². Fig. 4b illustrates the microphotographs of the texture seen under POM in the absence of field where as Figs. 4c and 4d show the photomicrographs of the microscopic textural changes observed under the applied electric field. Similar results were obtained when the SmC* phase of sample **SA(3R)-11** was subjected to electric filed study at 144 °C [65.4 Vrms, (185 V) 30 Hz; 09 kΩ; P_s = 96 nC cm⁻²; see Figs. 4e-h]. The occurrence of single peak in both the samples suggests the ferroelectric behaviour of the mesophase investigated.

II.3. Circular dichroism

It is well known that the circular dichroism (CD) activity would be experiential when the optically active medium absorbs left and right hand circular polarized light (CPL) differently. The N* and SmC* phases, owing to their defect free helical superstructure, exhibit circular CD phenomenon wherein the incident light is resolved into its two circularly polarized (CP) components, left and right, at a given wavelength. In fact, at this wavelength, depending upon the helical sense (chirality) of the phase, the CPL of a particular handedness is completely reflected while its counterpart is transmitted. That is, the N* / SmC* phase shows CD at a given wavelength band where the incident unpolarized light beam (with equal amount of left and right handed CP components) will split into its right and left CP components. When white light propagates through a left-handed (LH) helix, the LH circularly polarized component with wavelength of the helix pitch is selectively reflected whereas the right-handed (RH) component is wholly transmitted. That is to say the reflected light is circularly polarized with the same handedness as that of the helix while the transmitted light possess opposite handedness. Thus, the helical handedness (screw sense) of the N* / SmC* phase formed by a pair of enantiomers, are opposite to each other. Accordingly, the CD

spectra recorded for the N* / SmC* phase of a pair of enantiomers (mirror-image isomers) are usually quasiperfect mirror images. In recent times, we have been focusing on such CD studies not only to substantiate the aforesaid aspects but also to point out what happens to the helix sense of the N* and SmC* phases when they exist in sequence.^{36,37} In continuation of such investigations, we examined the chiroptical property of the N* and SmC* phases formed by two pairs of enantiomers viz., **SB(3S)-9** & **SB(3R)-9** and **SA(3S)-9** & **SA(3R)-9**. Precisely, these samples were subjected to circular dichroism study.

As described in the following, the CD experiments performed in the present study are purely qualitative given the fact that the pre-fabricated standard (commercial) cells of known thickness could not be used. That is, when the samples were tested using standard cells the saturation problems arose wherein highly intense CD peaks emerged beyond the quantifiable range of the instrument. Therefore, very thin-films of the samples, **SB(3S)-9** / **SB(3R)-9** / **SA(3S)-9** / **SA(3R)-9**, were fabricated for the study. A tiny amount of mesogens (say 2-3 mg) sandwiched between the untreated quartz plates were heated to their isotropic phase and pressed hard frequently so as to obtain thin-films where the uniform spreading of samples throughout the cell is ensured. In the isotropic state, the spectra of the samples were recorded where CD activity, unlike in the SmC* and N* phases, was found to be insignificantly small implying that the chromophores are not affected by the molecular chirality, but they are indeed influenced by the chirality of the fluid phase. The samples from their isotropic melt were then cooled slowly, and the CD spectra were recorded, where the light path remains perpendicular to the sample surface, as a function of temperature, in the entire thermal range of the N* and SmC* phases sequentially. As anticipated, both the phases showed reliable and definite CD signals (Fig. 5). Apparently, the intensity of the signals increases with decrease in temperature implying the higher mobility of the flexible units of mesogens. The origin of the CD bands of the mesophases was authenticated by recording at four and six different orientations achieved by in-plane rotation of the samples by 90° and 60° respectively. The spectra obtained for all these orientations of the samples were found to be nearly identical to those obtained in the pristine orientation. Besides, the CD instrument employed in the present study has a built in ability to measure the LD directly. Thus, both LC phases were subjected to direct LD measurement where the activity was found to be zero. These results clearly infer that the observed CD activity of the mesophases is genuine and certainly not stemming from the possible linear dichroism (LD) artifact.

As can be seen in Figs. 5a & 5c and 5e & 5g, the CD spectra of the N* phase obtained for enantiomers **SB(3S)-9** & **SB(3R)-9** and **SA(3S)-9** & **SA(3R)-9** respectively exhibit an excellent mirror-image relationship over their entire thermal range. Likewise, CD spectra of the SmC* phase registered for the enantiomers **SB(3S)-9** & **SB(3R)-9** and **SA(3S)-9** & **SA(3R)-9** (Figs 5b & 5d and Figs. 5f & 5h) show quasi-mirror imaged CD pattern where multiple CD signals in each spectrum can be seen; the origin of such multiple bands points to different excitonically coupled chromophores capable of exhibiting several electronic transitions. Interestingly, the CD band at the wavelength (λ) \sim 400 nm obtained in the N* phase of **SB(3S)-9** is opposite (-ve) (Fig. 5a) to that of the +ve CD band observed at \sim 400 nm for the SmC* phase (Fig.5b) of the same sample under the same experimental conditions; the similar behavior can be seen in Figs. 5c & 5d, Figs. 5e & 5f and Figs. 5g & 5h belonging to the N* and SmC* phases of mesogens **SB(3R)-9**, **SA(3S)-9** and **SA(3R)-9** respectively. These observations imply that the N* and SmC* structures derived from an enantiomer possess opposite helix-sense. Precisely, the reversal of the helix-sense (from right to left and vice-versa) happens during the N* to SmC* phase transition. In essence, the screw sense of the helical array of the N* phase and the SmC* phase of an enantiomer is opposite.

III. Conclusions

The synthesis and thermal behavior of twenty new three-ring ferroelectric calamitics, belonging to four different series, possessing a chiral tail at one end and an *n*-alkoxy chain at the other ending, have been reported. In particular, five pairs of enantiomeric Schiff bases as well as five pairs of optical isomers comprising salicylaldehyde-core have been investigated. Given the fact that they are derived from (3S)-3,7-dimethyloctyloxy and (3R)-3,7-dimethyloctyloxy tails, in a given pair of enantiomers the configuration of a chiral centre in one isomer is opposite to that of the corresponding centre in the other isomer. In each series, the length of the *n*-alkoxy tail has been varied from *n*-octyloxy to *n*-dodecyloxy especially to pursue the structure–property relationships. Notably, all the mesogens realized show thermodynamically stable SmC* phase apart from the BPI/II and N* phases. However, out of the ten Schiff bases (five pairs of enantiomers) realized, eight (four enantiomeric pairs) mesogens stabilize an additional metastable smectic (SmX) phase whose characteristics could not be revealed precisely. Generally, within a series, the isotropic melting temperatures as well as the thermal width of N* and SmC* phases decrease as the length of the *n*-alkoxy tail increases. The SmC*, N* and BPI/II phases exist over a thermal range of 80 - 115 °, 12 - 30 °

and $0.3 - 0.7^\circ$ respectively. The thermal width of the SmC* phase, when compared to other LC phases, is especially noteworthy for the prime reason that it shows ferroelectric switching characteristics with P_s value in the range of 69 - 96 nC/cm². CD spectroscopic technique has been used to determine the helix handedness (twist sense) of the SmC* and the N* phases formed by two pairs of enantiomers, as representative cases, each pair chosen from Schiff base and salicylaldimine series of compounds. In fact, the thin films of the samples show strong CD bands in entire thermal width of both N* and SmC* phases implying the presence of chromophores in a macroscopic chiral environment. As expected, the CD spectra obtained for the N* / SmC* phase of a pair enantiomers exhibited mirror-image patterns confirm optical isomeric relationships. Interestingly, the CD measurements also evidenced the helix handedness (helix-twist sense) of the N* phase being opposite to that of the SmC* phase. That is, a helix-twist sense inversion occurs when the N* phase transforms into the SmC* phase in a sequence. Overall, the three-ring chiral calamitic LCs reported herein are quite promising as they stabilize the technologically significant SmC* phase over a wide thermal range. We are continuing our studies in this direction so as to realize analogous systems displaying ferroelectric SmC* phase at room temperature with other properties required for technological application.

IV. Experimental

IV.1. General Information

Chemicals and solvents: The requisite chemicals/reagents and analytical grade solvents were procured from overseas as well as local companies. Whereas the bulk solvents used for purification/extraction and other general purposes were purchased from the local sources. Unless otherwise specified, chemicals/reagents were used as received from the suppliers without further purification. The bulk solvents prior to use were purified following the standard distillation methods.

Monitoring and purification: Thin layer chromatography (TLC) technique was used not only to monitor the progress and completion of reactions but also to evaluate the purity of the materials. TLC plates derived from aluminium sheets pre-coated with silica gel (Merck, Kieselgel60, F254) were used. Silica gel of mesh size 60-120, 100-200 and 230-400 was used as stationary phases in column chromatography technique.

Molecular structural characterization: In general, the target liquid crystalline materials and their intermediates were characterized structurally with the aid of UV-Vis, FTIR and NMR techniques. Electronic absorption (UV-Vis) spectroscopy was performed using a Perkin Elmer's, Lambda 20 UV-Vis spectrometer. IR spectra were recorded on a PerkinElmer Spectrum 1000 FT-IR spectrometer; the spectral positions are given in wave number (cm^{-1}) unit. Proton (^1H) and carbon (^{13}C) NMR spectra were recorded in CDCl_3 on Bruker AMX-400 (400 MHz) spectrometer at ambient temperature; the chemical shifts (δ) are reported in parts per million (ppm) relative to the chemical shift of tetramethylsilane (TMS) as an internal standard; coupling constants (J) are given in Hz. Mass spectra of the target compounds were recorded on JEOL JMS-600H spectrometer (Tokyo, Japan) in FAB+ mode using 3-nitrobenzyl alcohol as a liquid matrix. Elemental microanalysis data of the final compounds was obtained from the PerkinElmer 2400 Series II. CHNS/O Elemental Analyzer.

Mesomorphic and chiroptical behavior: The liquid crystal properties of the mesogens were revealed with the aid of an Olympus BX50; Model BX50F4 optical polarizing microscope, attached to a digital camera and a Mettler FP82HT hot stage programmed by an FP90 Central Processor, and differential scanning calorimeter (DSC) (Perkin-Elmer Diamond DSC with the PC system operating on Pyris software). The DSC instrument prior to sample measurement was calibrated using pure indium as a standard. DSC traces recorded at a scanning rate of $5\text{ }^\circ\text{C}/\text{min}$ were employed to determine the transition temperatures and associated enthalpies. X-Ray diffraction (XRD) studies with $\text{CuK}\alpha$ ($\lambda = 0.15418\text{ nm}$) radiation were carried out using a powder X-ray diffractometer viz., PANalytical X'Pert PRO MP machine consisting of a focusing elliptical mirror and a fast resolution detector (PIXCEL). The samples under XRD investigation were filled in Lindemann capillaries (0.5 mm diameter) in their isotropic state by capillary action and both ends of the capillaries were flame sealed carefully. The diffraction patterns were recorded at chosen temperatures with a diffraction angle between 0 and 32° . Specific rotation of the compounds was measured using Rudolph AUTOPOL IV Automatic Polarimeter. CD spectra were recorded with the aid of Jasco J-810 spectropolarimeter.

IV.2. Synthetic procedures and characterization

General procedure for the synthesis of calamitics belonging to **Series-I: SB(3S)-n**, **Series-II: SB(3R)-n**, **Series-III: SA-(3S)-n** and **Series-IV: SA-(3R)-n**.

A mixture of 4-formylphenyl 4-(*n*-alkoxy)benzoate (**7a-e**) / 4-formyl-3-hydroxyphenyl 4-(*n*-alkoxy)benzoate (0.33 mmol, 1 eq.) (**8a-e**) and (*S*)-4-((3,7-dimethyloctyl)-oxy)aniline (**3**) / (*R*)-4-((3,7-dimethyloctyl)oxy)aniline (**4**) (0.4 mmol, 1.2 eq.), catalytic amount of acetic acid in ethanol (10 mL) was refluxed under inert atmosphere for 2 h. The solid separated upon cooling the reaction mixture was collected by filtration, washed with ethanol and air-dried. The crude product was purified by repeated recrystallizations using absolute ethanol (Yields: Schiff bases, 82-86% and salicylaldimes, 80-86%).

In the following molecular structural characterization data are given for a member of Schiff base series and that of a salicylaldimine series, as representative cases, while the analytical data for other compounds are detailed in the Supporting Information.

SB(3S)-8: a white solid; yield: 0.201 g (86%); $[\alpha]_{\text{D}}^{25}$ - 6.8 (1 %, CHCl₃); IR (KBr pellet): ν_{max} in cm⁻¹ 2922, 2851, 1738, 1608, 1511, 1468 and 1163; UV-Vis: λ_{max} = 340.97 nm, ϵ = 1.9971 × 10⁻² L mol⁻¹ cm⁻¹; ¹H NMR (400MHz, CDCl₃): δ 8.49 (s, 1H, 1 × CH=N), 8.16 (d, *J* = 9.2 Hz, 2H, Ar), 7.96 (d, *J* = 8.4 Hz, 2H, Ar), 7.33 (d, *J* = 8.8 Hz, 2H, Ar), 7.24 (d, *J* = 8.8 Hz, 2H, Ar), 6.99 (d, *J* = 8.8 Hz, 2H, Ar), 6.94 (d, *J* = 8.8 Hz, 1H Ar), 4.06 (t, *J* = 6.4 Hz, 2H, 1 × OCH₂), 3.99 (m, 1H, 1 × -CH-), 1.87-0.87 (m, 33H, 1 × CH, 10 × CH₂, 4 × CH₃); ¹³C NMR (100MHz): 164.62, 163.69, 157.93, 157.03, 153.21, 144.60, 134.09, 132.34, 129.71, 122.18, 122.17, 121.28, 115.02, 114.36, 68.37, 66.64, 39.25, 37.31, 36.25, 31.79, 29.88, 29.31, 29.21, 29.09, 27.97, 25.98, 24.66, 22.70, 22.64, 22.60, 19.68, 14.08. MS(FAB⁺): *m/z* Calcd. for C₃₈H₅₁NO₄:(M+2) 587.82; Found: 588.06; Anal. calcd for C₃₈H₅₁NO₄: C, 77.91; H, 8.77; N, 2.39. Found: C, 77.68; H, 8.73; N, 2.53.

SA(3S)-8: a pale yellow solid; yield: 0.205 g (85%); $[\alpha]_{\text{D}}^{25}$ - 6.3 (1 %, CHCl₃); IR (KBr pellet): ν_{max} in cm⁻¹ 2951, 2925, 2857, 1722, 1604, 1510, 1467 and 1170; UV-Vis: λ_{max} = 352.25 nm, ϵ = 1.1621 × 10⁻² L mol⁻¹ cm⁻¹; ¹H NMR (400MHz, CDCl₃): δ 13.79 (s, 1H, Ar-OH), 8.61 (s, 1H, 1 × CH=N), 8.15 (d, *J* = 8.8 Hz, 2H, Ar), 7.41 (d, *J* = 8.4 Hz, 1H, Ar), 7.28 (d, *J* = 8.8 Hz, 2H, Ar), 6.98 (d, *J* = 8.8 Hz, 2H, Ar), 6.96 (d, *J* = 8.8 Hz, 2H, Ar), 6.88 (d, *J* = 8.8 Hz, 1H Ar), 6.83 (dd, *J*₁ = 8.4 Hz, *J*₂ = 2 Hz, 1H Ar), 4.06 (m, 4H, 2 × OCH₂), 4.00 (m, 1H, 1 × -CH-), 1.89-0.87 (m, 33H, 1 × CH, 10 × CH₂, 4 × CH₃); ¹³C NMR (100MHz): 164.41, 163.68, 162.44, 159.42, 158.48, 140.93, 132.72, 132.36, 122.23, 121.29, 117.32,

115.24, 114.35, 112.93, 110.54, 68.37, 66.70, 39.24, 37.29, 36.19, 31.79, 29.87, 29.31, 29.20, 29.09, 27.97, 25.98, 24.65, 22.69, 22.64, 22.59, 19.67, 14.08. MS(FAB⁺): m/z Calcd. for C₃₈H₅₁NO₅: 601.815; Found: 603.29; Anal. calcd for C₃₈H₅₁NO₅: C, 75.84; H, 8.54; N, 2.33. Found: C, 75.67; H, 8.61; N, 2.36.

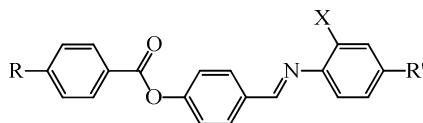
Acknowledgements: CVY sincerely thank the Department of Science and Technology (DST), New Delhi, Govt. of India, for financial support through SERB project No. EMR/2017/S1/000153. The authors thank Mrs. Srividhya Parthasarathi for her help while carrying out electrical switching studies.

References

1. H. Yamamoto, E. Carreira, *Comprehensive Chirality*, 1st Edition, Elsevier Science, Amsterdam, **2012**.
2. A. Guijarro, Y. Miguel, *The Origin of Chirality in the Molecules of Life: A Revision from Awareness to the Current Theories and Perspectives of this Unsolved Problem*, **2009**, RSC Publishing.
3. (a) M. M. Green, R. J. M. Nolte, E. W. Meijer (Eds.), *Materials Chirality: Volume 24 of Topics in Stereochemistry*, **2003**, John Wiley & Sons Inc., New Jersey;
4. (a) J. W. Goodby, P. J. Collings, T. Kato, C. Tschierske, H. Gleeson, P. Raynes, (Editors). *Handbook of Liquid Crystals; Volume 1: Fundamentals of Liquid Crystals. Part-II; Symmetry and Chirality in Liquid Crystals*, 2nd Edition, **2014**, Weinheim, Wiley-VCH. (b) J. Fan, Y. Li, H. K. Bisoyi, R. S. Zola, D. Yang, T. J. Bunning, D. A. Weitz, Q. Li, *Angew. Chem. Int. Ed.* **2015**, *54*, 2160-2164. (c) H. K. Bisoyi, Q. Li, *Angew. Chem. Int. Ed.* **2016**, *55*, 2994-3010. (d) Z. -G. Zheng, C. -L. Yuan, W. Hu, H. K. Bisoyi, M. -J. Tang, Z. Liu, P. -Z. Sun, W. -Q. Yang, X. -Q. Wang, D. Shen, Y. Li, F. Ye, Y. -Q. Lu, G. Li, Q. Li, *Adv. Mater.* **2017**, *29*, 1703165. (e) Z. -G. Zheng, Y. Li, H. K. Bisoyi, L. Wang, T. J. Bunning, Q. Li, *Nature*, **2016**, *531*, 352-356.
5. I. Dierking, *Symmetry*, **2014**, *6*, 444-472
6. H.-S. Kitzerow, C. Bahr (Eds). *Chirality in Liquid Crystals*, **2001**, Springer-Verlag New York, Inc.
7. P. J. Collings, J. S. Patel (Eds.), *Handbook of Liquid Crystal Research*, **1997**, Oxford University press.
8. R. B. Meyer, *Mol. Cryst. Liq. Cryst.*, **1977**, *40*, 33-48

9. J. W. Goodby, P. J. Collings, T. Kato, C. Tschierske, H. Gleeson, P. Raynes, P. (Editors). *Handbook of Liquid Crystals; Volume 4: Smectic and Columnar Liquid Crystals*, 2nd Edition, Weinheim, Wiley-VCH, **2014**.
10. S. T. Lagerwall, *Ferroelectric and Antiferroelectric Liquid Crystals*, **1999**, Wiley-VCH: Weinheim.
11. J. W. Goodby, R. Blinc, N. A. Clark, S.T. Lagerwall, M. A. Osipov, S.A. Pikin, T. Sakurai, K. Yoshino, B. Zeks, *Ferroelectric Liquid Crystals. Principle and Applications*, **1991**, Gordon and Breach: Philadelphia.
12. H. Takezoe, *Ferroelectric, Antiferroelectric and Ferrielectric Liquid Crystals: Applications, Encyclopedia of Materials: Science and Technology*, **2001**, Elsevier Science Ltd..
13. S. T. Lagerwall, 'Ferroelectric liquid crystals', in *Low molecular weight liquid crystals II*, Vol. 2B, eds. D. Demus, J. Goodby, G. W. Gray, H.-W. Spiess and V. Vill, **1998**, Wiley-VCH, Weinheim, pp. 515–664.
14. A. S. Tayi, A. Kaeser, M. Matsumoto, T. Aida, S. I. Stupp, *Nat. Chem.*, **2015**, 7, 281-294.
15. M. Lallart, M. (Ed), *Ferroelectrics - Physical Effects*; Chapter 17 by S. Pirkl, M. Glogarova, "*Ferroelectric Liquid Crystals with High Spontaneous Polarization*, **2011**.
16. I. Musevic, R. Blinc, B. Zeks, *The Physics of Ferroelectric and Antiferroelectric Liquid Crystals*, **2000**, World Scientific, Singapore.
17. I. Dierking, *Materials*, **2014**, 7, 3568-3587.
18. M. A. Osipov, M. V. Gorkunov, *Liq. Cryst.*, **2009**, 36, 1281–1288
19. S.T. Lagerwall, *Ferroelectrics*, **2004**, 301, 15-45.
20. S. J. J. Elston, *Mod. Optics*, **1995**, 42, 19-56.
21. J. W. Goodby, *J. Mater. Chem.* **1991**, 1, 307-318.
22. S. M. Kelly, R. Buchecker, M. Schadt, *Liq. Cryst.*, **1988**, 3, 1125-1128.
23. M. Hird, *Liq. Cryst.*, **2011**, 38, 1467-1493.
24. C.-H. Lin, *Int. J. Mol. Sci.*, **2013**, 14, 21306-21318
25. M. Subrao, D. M. Potukuchi, G. S. Ramachandra, P. Bhagavath, S. G. Bhat, S. Maddasani, *Beilstein J. Org. Chem.*, **2015**, 11, 233–241.
26. A. D. L. Chandani, Y. Ouchi, H. Takezoe, A. Fukuda, *Jpn. J. Appl. Phys.* **1989**, 28, L1261–L1264.

27. I. A. Radini, M. Hird, *Liq. Cryst.*, **2009**, *36*, 1417-1430 and references cited therein.
28. S. M. Kelly, *Helv. Chimica Acta*, **1889**, *72*, 594-607.
29. J. Thisayukta, E. T. Samulski, *J. Mater. Chem.*, **2004**, *14*, 1554-1559.
30. N. Kasthuraiah, B. K. Sadashiva, S. Krishna Prasad, G. G. Nair, *Liq. Cryst.*, **1998**, *24*, 639-645.
31. J. S. Dave, M. R. Menon, P. R. Patel, *Mol. Cryst. Liq. Cryst.*, **2001**, *364*, 575-587.
32. J. W. Goodby, A. Petrenko, M. Hird, R. A. Lewis, J. Meier, J. C. Jones, *Chem. Commun.*, **2000**, 1149-1150.
33. V. Faye, J. C. Rouillon, H. T. Nguyen, L. Detre, V. Laux, N. Isaert, *Liq. Cryst.* **1998**, *24*, 747-758.
34. S. J. Cowling, A. W. Hall, J. W. Goodby, *Liq. Cryst.* **2005**, *32*, 1483-1498.
35. M. Hird, *Chem. Soc. Rev.*, **2007**, *36*, 2070-2095.
36. B. N. Veerabhadraswamy, D. S. Shankar Rao, C. V. Yelamaggad. *J. Phy. Chem. B.*, **2015**, *119*, 4539-4551.
37. B. N. Veerabhadraswamy, D. S. Shankar Rao, S. Krishna Prasad, C. V. Yelamaggad. *New J. Chem.*, **2015**, *39*, 2011-2027.
38. I. Dierking, *Textures of Liquid Crystals*, **2003**, Wiley-VCH Verlag GmbH & Co. KGaA,



Schiff bases: X = H

R' = (*S*)-Octyloxy / R' = (*R*)-Octyloxy

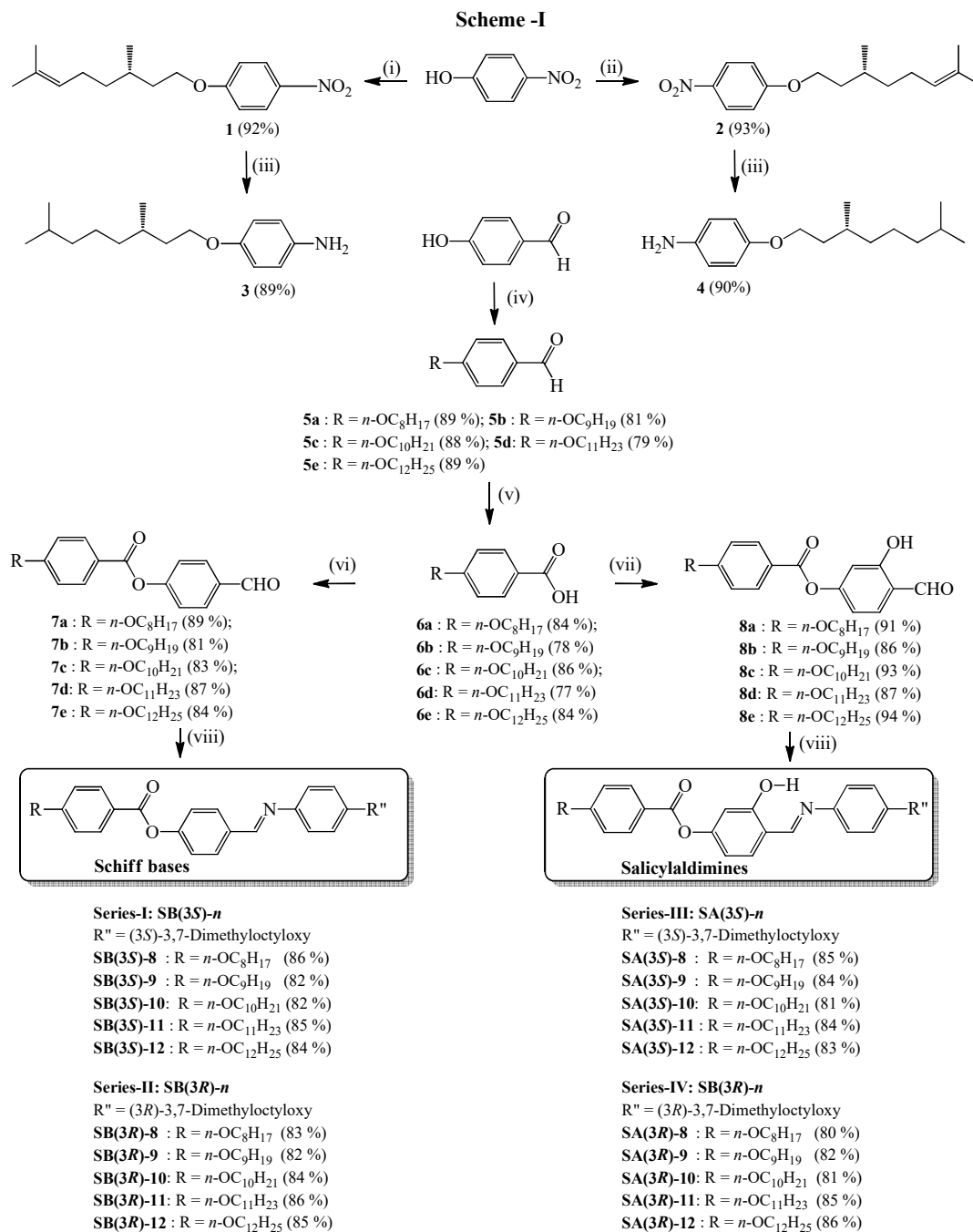
R = OC₈H₁₇; OC₉H₁₉; OC₁₀H₂₁; OC₁₁H₂₃; OC₁₂H₂₅

Salicylaldimines: X = OH

R' = (*S*)-Octyloxy / R' = (*R*)-Octyloxy

R = OC₈H₁₇; OC₉H₁₉; OC₁₀H₂₁; OC₁₁H₂₃; OC₁₂H₂₅

Chart 1: The molecular structure of ferroelectric Schiff bases and salicylaldimines investigated in the previous studies (see Ref. 36 and 37)



Reagents and conditions: (i) (*R*)-(-)-Citronellyl bromide, anhyd. K₂CO₃, KI, Butanone, reflux, 12 h. (ii) (*S*)-(+)-Citronellyl bromide, anhyd. K₂CO₃, KI, Butanone, reflux, 12 h. (iii) H₂ (1 atm, balloon), 10 % Pd-C, THF, rt, 4 h. (iv) *n*-Bromoalkanes, anhydrous K₂CO₃, DMF, 80 °C, 12 h. (v) Jones reagent, acetone, rt, 1 h. (vi) 4-Hydroxybenzaldehyds or 2,4-dihydroxybenzaldehyde, DCC, DMAP, THF, rt, 4 h. (vii) 2,4-Dihydroxybenzaldehyde, DCC, DMAP, THF, rt, 4 h. (viii) **3** or **4**, EtOH, AcOH, reflux, 5 h.

Table 1. Phase transition temperatures ($^{\circ}\text{C}$)^a and associated enthalpies (kJ/mol^{-1}) of transitions noted for three-ring rod-like Series-I, **SB(3S)-*n***, and Series-II, **SB(3R)-*n***, series of compounds. • = Enantiotropic phase; (•) = Monotropic LC phase. Cr: Crystal; SmX : Unknown smectic phase; SmC*: Chiral smectic C phase; N* : Chiral nematic phase; BP = Blue phase-I or Blue phase-II.

LCs	Cr	Heating Cooling	SmX	Heating Cooling	SmC*	Heating Cooling	N*	Heating Cooling	BP	Heating Cooling	I
SB(3S)-8	•	87.9 [46.9] 62.7 [11.5]	(•)	- 64.5 [24.2]	•	152.5 [2.8] 151.5 [2.8]	•	177.4 [1.6] 176.4 [1.5] ^b	•	- 176.9	•
SB(3R)-8	•	88.1 [46.9] 63.4 [11.5]	(•)	- 66.8 [24.2]	•	153.1 [2.8] 151.9 [2.8]	•	177.9 [1.6] 177.2 [1.5] ^b	•	- 177.5	•
SB(3S)-9	•	83.3 [74.2] 57.7 [32.4]	(•)	- -	•	154.9 [3.7] 153.7 [3.6]	•	173.9 [2.0] 172.7 [1.6] ^b	•	- 173.2	•
SB(3R)-9	•	83.5 [74.2] 57.6 [32.4]	(•)	- -	•	154.5 [3.7] 153.4 [3.6]	•	173.4 [2.0] 172.6 [1.6] ^b	•	- 173.1	•
SB(3S)-10	•	85.4 [74.1] 50.1 [47.0]	(•)	- 62.8 [7.2]	•	156.2 [3.8] 155.3 [3.8]	•	171.0 [1.7] 170.3 [1.8] ^b	•	- 170.9	•
SB(3R)-10	•	85.9 [74.1] ^c 52.1 [47.0]	(•)	- 62.4 [7.2]	•	156.0 [3.8] 154.7 [3.8]	•	171.0 [1.7] 170.0 [1.8] ^b	•	- 170.6	•
SB(3S)-11	•	86.9 [85.3] 50.1 [51.1]	(•)	- 68.0 [10.5]	•	156.9 [1.1] 156.0 [5.3]	•	168.2 [1.0] 167.3 [2.5] ^b	•	- 167.8	•
SB(3R)-11	•	86.1 [85.3] 50.1 [51.1]	(•)	- 67.6 [10.5]	•	156.4 [1.1] 155.6 [5.3]	•	167.7 [1.0] 167.0 [2.5] ^b	•	- 167.5	•
SB(3S)-12	•	74.6 [69.2] -	(•)	- 72.6 [7.8] ^d	•	159.0 [4.3] 157.0 [4.3]	•	166.9 [2.0] 165.8 [1.9] ^b	•	- 166.2	•
SB(3R)-12	•	73.9 [69.2] -	(•)	- 72.6 [7.8] ^d	•	156.7 [4.3] 155.8 [4.3]	•	165.5 [2.0] 164.8 [1.9] ^b	•	- 165.2	•

^a Transition temperatures determined by both polarizing optical microscope (POM) and peak values of the DSC traces during the first heating/cooling cycles at $5^{\circ}\text{C}/\text{min}$ rate. ^b The I-BP and BP-N* phase transitions were seen under POM, but they were too weak to be detected by DSC; thus, the ΔH value represents the combined enthalpy for the I-BP and BP-N* transitions. ^c The SmX phase freezes into a glassy state near room temperature ($\sim 30^{\circ}\text{C}$) that remains unaltered till -50°C (limitation of the instrument).

Table 2: Phase sequences, phase transition temperatures (°C)^a and associated enthalpies (kJ/mol-1) of transitions of three-ring rod-like Series-III, **SA(3S)-*n*** and Series-IV, **SA(3R)-*n*** compounds. • = Enantiotropic phase; Cr: Crystal; SmC*: Chiral smectic C phase; N*: Chiral nematic phase; BP = Blue phase-I or Blue phase-II.

LCs	Cr	Heating Cooling	SmC*	Heating Cooling	N*	Heating Cooling	BP	Heating Cooling	I
SA(3S)-8	•	80.7 [44.4] 35.0 [25.9]	•	152.5 [4.7] 150.0 [4.7]	•	181.8 [1.6] 180.0 [1.9] ^b	•	- 180.3	•
SA(3R)-8	•	80.1 [43.1] 33.5 [24.8]	•	152.5 [4.5] 150.2 [4.7]	•	181.8 [1.5] 180.0 [1.8] ^b	•	- 180.2	•
SA(3S)-9	•	77.1 [40.0] 51.4 [31.3]	•	154.9 [5.5] 152.6 [5.4]	•	176.8 [1.5] 175.0 [1.9] ^b	•	- 175.5	•
SA(3R)-9	•	76.4 [36.0] 51.4 [31.2]	•	154.8 [5.4] 152.5 [5.2]	•	176.7 [1.4] 175.1 [1.9] ^b	•	- 175.4	•
SA(3S)-10	•	84.0 [38.2] 58.3 [31.7]	•	158.0 [6.1] 154.7 [5.7]	•	176.3 [1.4] 174.0 [2.0] ^b	•	- 174.6	•
SA(3R)-10	•	84.2 [37.3] 58.4 [31.6]	•	158.1 [6.0] 154.5 [5.6]	•	176.4 [1.2] 174.1 [1.8] ^b	•	- 174.5	•
SA(3S)-11	•	89.6 [46.3] 62.8 [38.6]	•	159.8 [6.3] 157.7 [6.2]	•	174.0 [1.7] 172.4 [1.9] ^b	•	- 172.8	•
SA(3R)-11	•	89.3 [46.5] 62.6 [38.5]	•	159.8 [6.2] 157.5 [6.3]	•	174.1 [1.7] 172.2 [1.8] ^b	•	- 172.6	•
SA(3S)-12	•	91.2 [46.0] 65.8 [39.3]	•	160.1 [6.6] 158.4 [6.6]	•	171.5 [2.1] 170.2 [1.8] ^b	•	- 170.9	•
SA(3R)-12	•	90.5 [39.5] 65.8 [39.0]	•	160.1 [6.4] 158.3 [6.4]	•	171.5 [2.1] 170.3 [1.8] ^b	•	- 170.9	•

^a Peak temperatures in the DSC traces obtained during the first heating-cooling cycles at 5 °C / min. rate. ^b The I-BP and BP-N* phase transitions were seen under POM, but they were too weak to be detected by DSC; thus, the ΔH value represents the combined enthalpy for the I-BP and BP-N* transitions.

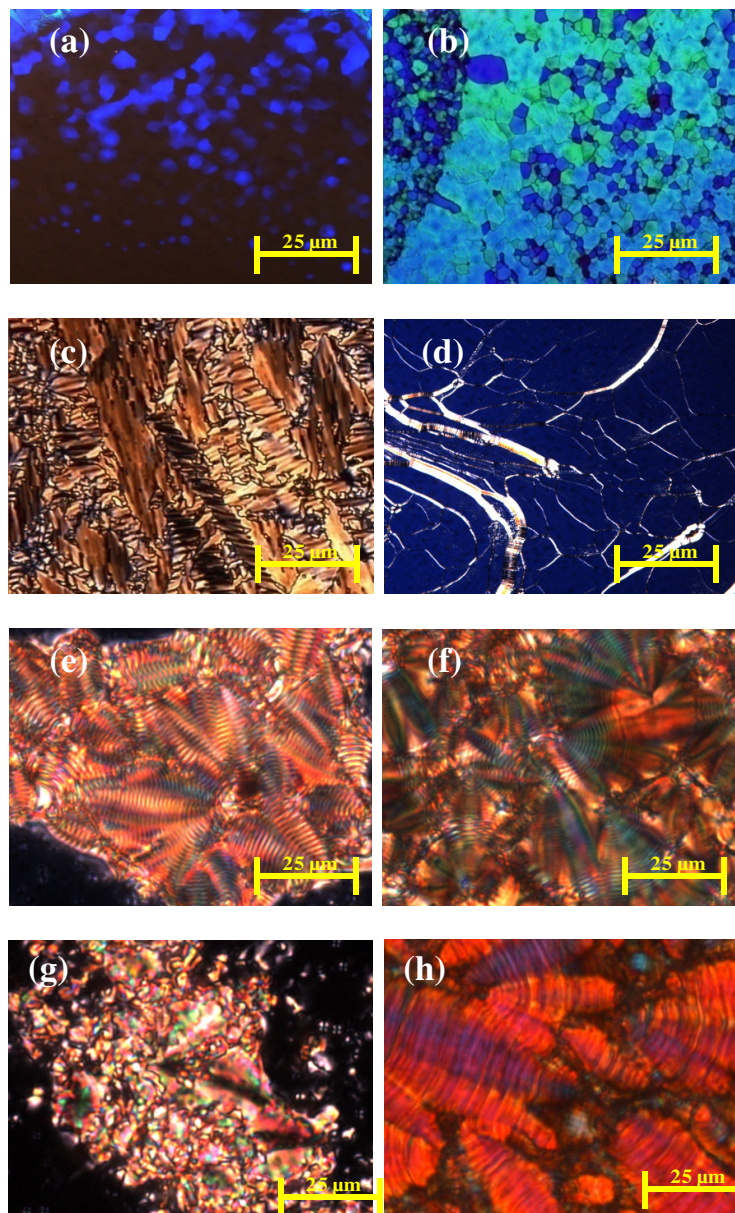


Figure 1. Microphotographs of optical textures of the liquid crystal phases exhibited by mesogens **SB(3S)-12** and **SA(3R)-10**. (a) The platelet texture of the BP-I/II seen (at 166.2 °C) just growing from the dark-blue background of BPIII of compound **SB(3S)-12**. (b) A completely grown textural pattern of the BP-I/II featuring platelets observed for the mesogen **SA(3R)-10** at 174.2 °C. (c) The fan-shaped or fan-like texture observed for the N* phase of mesogen **SB(3S)-12** at 164 °C. (d) The oily streaks texture of the planarly aligned N* phase formed after shearing the fan-shaped pattern of sample **SA(3R)-10** (160 °C). (e) Banded broken focal-conic pattern and the intense dark-greyish texture seen for the planarly and homeotropically oriented SmC* phase respectively for the compound **SB(3S)-12** (140 °C). (f) A striking banded broken focal-conic textural pattern observed at 152.4 °C for the SmC* phase of mesogen **SA(3R)-10** placed between the slides treated for planar alignment. (g) The texture observed for the SmX phase of compound **SB(3S)-12** at 65 °C. (h) An unfamiliar texture seen at 65 °C for the SmX phase of the sample **SB(3S)-12** examined in slides treated for planar orientation.

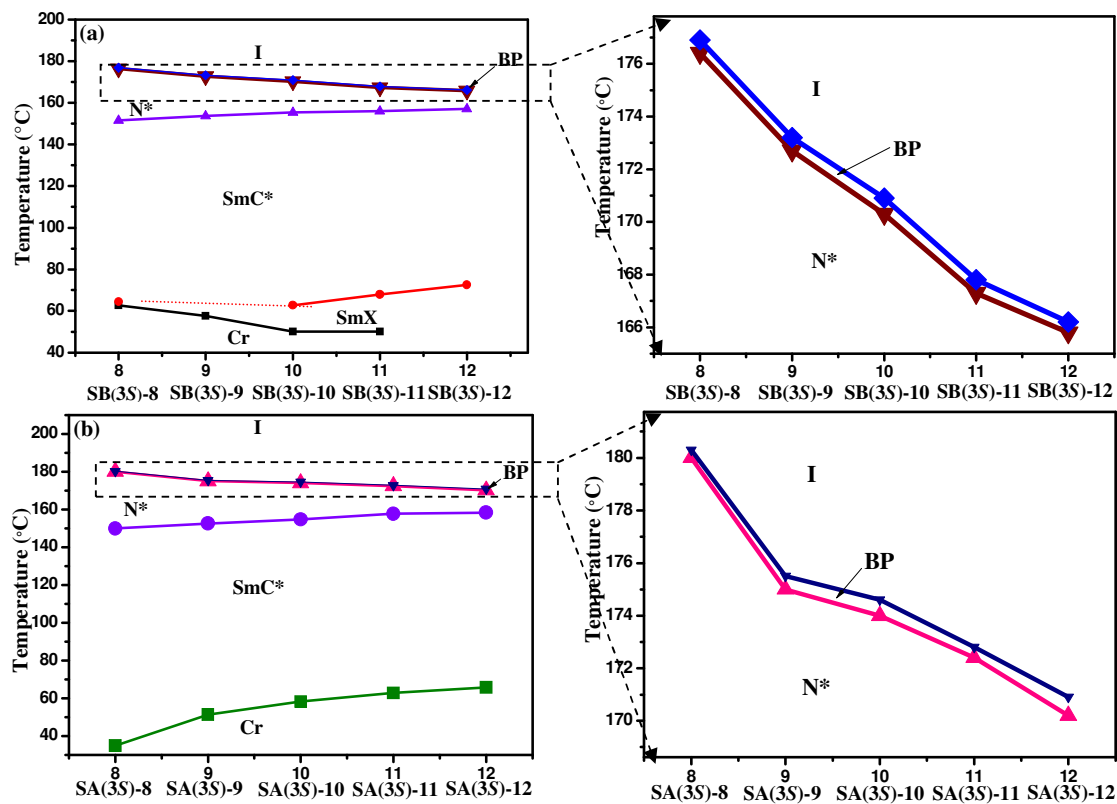


Figure 2. Plots of transition temperatures of the cooling cycle as a function of the terminal n -alkoxy chain for mesogens belonging to Series-I; SB(3S)- n (a) and Series-III; SA(3S)- n (b). Dotted red line in profile (a) specify that the data for mesogen SB(3S)-9 is not available.

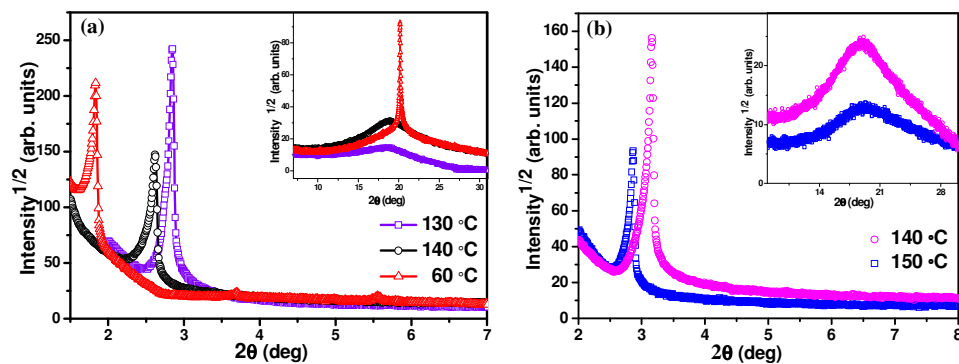


Figure 3. The 1D intensity versus 2θ XRD profiles recorded for the mesophases Schiff bases and salicylaldehydes: (a) The SmC* phase of **SB(3S)-8** (violet-trace) and **SB(3S)-12** (black-trace), and the SmX phase of **SB(3S)-12** (red-trace). (b) The SmC* phase of **SA(3S)-8** (pink trace) and **SA(3R)-12** (blue-trace). In all the profiles the inset shows a diffuse peak, seen in the wide angle region that confirms liquid-like ordering within the layer.

Table 3. XRD data of the chiral smectic C phase exhibited by mesogens **SB(3S)-8**, **SB(3S)-12**, **SA(3S)-8** and **SA(3R)-12**. The spacings (d) corresponding to the low-angle reflections, the wide-angle peak positions, the molecular length (L) in the most extended form with an all-*trans* conformation of the alkoxy chains, d/L ratio and tilt angle of the mesogens are also shown.

Mesogen (Molecular length / Å)	Temperature / °C	Layer spacing - d (low-angle peak position) / Å	Wide-angle peak position / Å	d/L	Tilt angle (θ) $= \cos^{-1}(d/L)$
SB(3S)-8 (42.33)	140	31.72	4.35	0.75	41.40
	130	30.99		0.73	43.11
	80	30.12		0.71	44.76
	50	27.89		0.66	48.70
SB(3S)-12 (47.59)	150	34.31	4.8	0.72	43.94
	140	33.66		0.71	44.76
	90	33.71		0.71	44.76
	80	34.05		0.72	43.94
	60	31.59		0.66	48.70
SA(3S)-8 (42.33)	140	30.59	4.80	0.72	43.94
	90	27.42		0.65	49.45
	60	27.37		0.65	49.94
SA(3R)-12 (47.61)	150	31.04	4.79	0.65	49.45
	100	30.06		0.63	50.94
	80	30.59		0.64	50.20

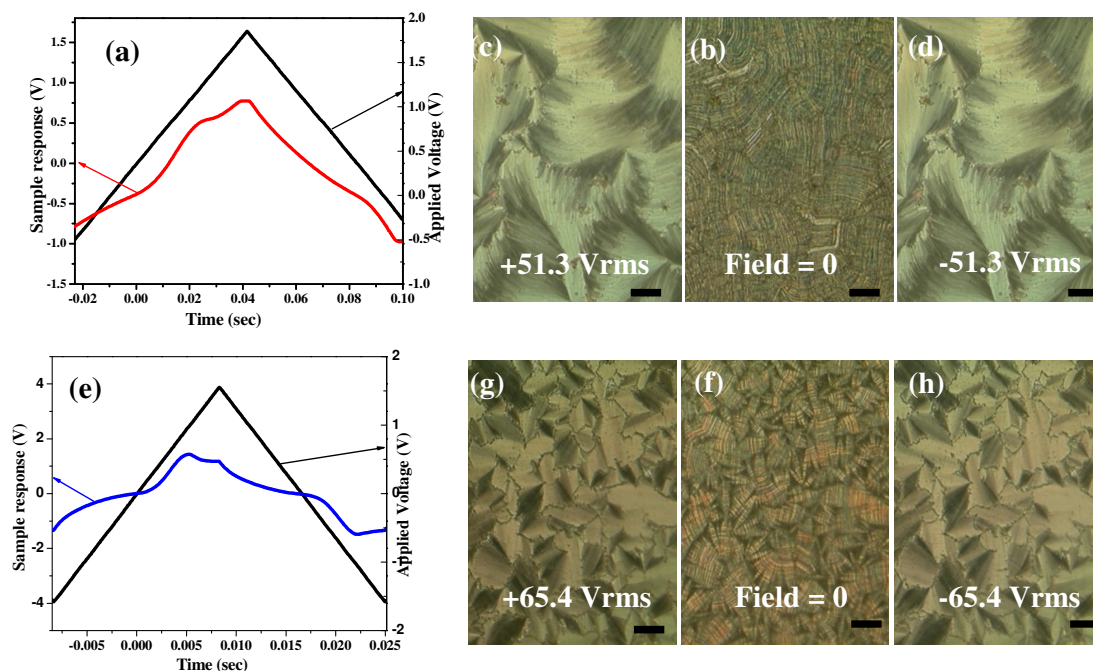


Figure 4. Switching current response peaks obtained upon applying a triangular-wave field for the SmC* phase of mesogens **SB(3S)-8** (129 °C; 145.3 V, 5 Hz; 09 kΩ; $P_s = 69 \text{ nC cm}^{-2}$) (a) and **SA(3R)-11**, (144 °C; 185 V, 30 Hz; 09 kΩ; $P_s = 96 \text{ nC cm}^{-2}$) (e). Microphotographs of the microscopic textural changes observed under the applied electric field (c,d & g,h) and in the absence of field (b & f) (Bar: 100 μm).

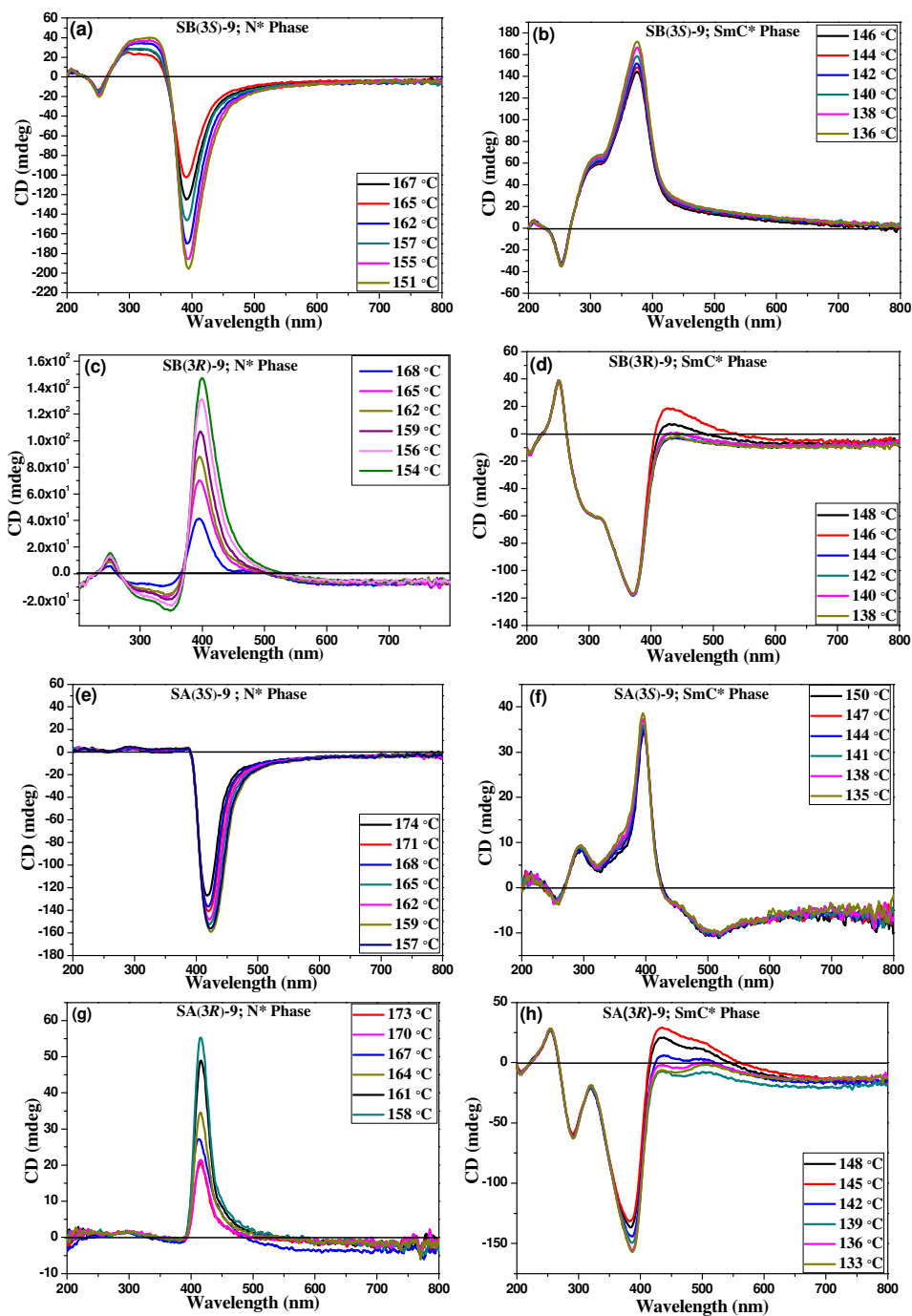


Figure 5. CD spectra obtained as a function of temperature in the N* (a & c and e & g) and SmC* (b & d and f & h) phases exhibited by the enantiomer SB(3S)-9 & SB(3R)-9 and SA(3S)-9 & SA(3R)-9.